

DOI: 10.1002/x0xx00000x

Copolymer derived micro/meso porous carbon nanofibers with vacancy-type defects for high-performance supercapacitors

Jiye Li¹, Weimiao Zhang¹, Xu Zhang¹, Liyao Huo¹, Jiayi Liang¹, Lisheng Wu¹, Yong Liu², Jiefeng Gao^{1*}, Huan Pang^{1*} and Huaiguo Xue^{1*}

1 School of Chemistry and Chemical Engineering, Yangzhou University, Yangzhou, 225009, Jiangsu, P. R. China.

2 Henan Key Laboratory of Non-Ferrous Materials Science & Processing Technology, Henan University of Science and Technology, Luoyang, China.

E-mail: huanpangchem@hotmail.com; panghuan@yzu.edu.cn; jfgao@yzu.edu.cn;
chhxue@yzu.edu.cn

Homepage: <http://huanpangchem.wix.com/advanced-material>

This PDF file includes:

Section S1. Materials and methods

Section S2. Electrochemical measurement

Section S3. Electrochemical Data

Fig. S1. Schematic diagram of P (AN-*co*-AA)/PTA fiber preparation process.

FT-IR spectrum of P(AN-*co*-AA).

Fig. S2. TEM images of B-CNF, C-CNF and fiber which formed without sublimating PTA.

Fig. S3. Thermogravimetric analysis.

Fig. S4. Additional SEM images of HPCNFs.

Fig. S5. Flexibility of HPCNFs.

Fig. S6. XPS spectra and contact angles.

Fig. S7. Galvanostatic charge/discharge curves.

Fig. S8. Capacitance contribution analyses.

Fig. S9. Impedance analysis.

Fig. S10. Electrochemical performance.

Table S1. The content of the elements in the copolymer.

Table S2. Summary of the physical and chemical characterization.

Table S3. Summary of the electrochemical capacitive performance.

References and notes

Section S1. Materials and methods

Materials

Monomer AN is analytical grade and distills to remove inhibitors. Comonomers AA is distilled to remove inhibitors via reduced pressure distillation. Azo-bis(isobutyronitrile) (AIBN) is recrystallized from ethanol and used as initiator. N, N-dimethylformamide (DMF; ≥99.7%), and dimethyl sulfoxide (DMSO; ≥99.9%) were purchased from Sinopharm Chemical ReagentCo., Ltd.

Preparation of P(AN-*co*-AA) by Free Radical Polymerization

30 ml mixture of AN and AA ($m_{AN} : m_{AA} = 53:6$) with different molar ratio together with AIBN was added to 150 ml of dimethyl sulfoxide (DMSO) in a 250 ml three-necked flask, and the polymerization reaction was carried out for 48 hours under mechanical stirring in a nitrogen atmosphere.

Preparation of HPCNFs

As shown in Fig.S1, P(AN-*co*-AA) copolymer and PTA ($M_{P(AN-co-AA)} : M_{PTA} = 8:5$) was dissolved in DMF at a concentration of 13 weight %. The solution was stirred at 80°C for several hours and then electrospun to polymer fiber mats at a feeding rate of 3 ml/hour under a voltage of 25 kV (TONG LI TECH Nanofiber Electrospinning Unit). The obtained copolymer nanofibrous membrane was subject to pre-oxidation at the temperature of 240 °C for 2 h, followed by calcination at 800 °C in a nitrogen atmosphere for 1 h. For comparison, PAN mixed with TPA and P(AN-*co*-AA) were electrospun into polymer fiber mats and underwent the identical pyrolysis steps at 800°C to obtain carbon fiber mats.

Section S2. Electrochemical measurement:

The working electrodes were fabricated by sandwiching carbon nanofibers between two pieces of titanium meshes without any conductive additives or polymer binders (area: $1 \times 1\text{cm}^2$, mass: approx. 1.5 mg). In the symmetric cells, two identical (by weight, size,

and composition) active-material electrodes were used as cathode and anode. Electrochemical performances of HPCNFs, including Cyclic voltammetry (CV) and Galvanostatic charge/discharge (GCD) and Electric impedance spectroscopy (EIS) were conducted using an electrochemical workstation (Interface5000E). Electric impedance spectroscopy (EIS) was performed with an amplitude of 10 mV and a frequency from 10 mHz to 100 kHz.

Section S3. Electrochemical Data

For a nonlinear Faradaic capacitor, the capacitance is obtained from the integrated form

$$C = \frac{\int dQ}{\int dV} = \frac{\int Idt}{\int dV} = \frac{i\Delta t}{\Delta V}$$

(1)

i is the average current during the charging or discharging, ΔV is the potential window, and Δt is the charging or discharging time.

(a) CV test

Since $dV/dt=v$ is a set constant (i.e., the scan rate), the discharge specific capacitance can be obtained by integrating the portion where the current is less than zero.

$$C = \frac{S}{v\Delta V}$$

(2)

Here $S = \int IdV$ is the loop area. The specific capacitance is the capacitance divided by the mass of the electrode.

$$C_m = \frac{S}{2mv\Delta V}$$

(3)

(b) GCD test

Since I is a set constant (i.e., the charging/discharging rate), $i=I$ so Eq (2) reduces to

$$C = \frac{I\Delta t}{\Delta V} \quad (4)$$

(For our Faradaic capacitance, the charging/discharging curves are rather linear, so $\Delta V/\Delta t$ is essentially the slope.) The specific capacitance is the capacitance divided by the mass of the electrode

$$C_m = \frac{I}{m(\Delta V/\Delta t)} \quad (5)$$

$$C_A = \frac{C_m}{A_{BET}}$$

The energy density and power density of device can be estimated using the following equations

$$E = 0.5C_m (V - V_{drop})^2 \quad (6)$$

$$P = \frac{E}{\Delta t} \quad (7)$$

V is the operating voltage, V_{drop} is obtained from the GCD test.

$$IR_{drop} = R_s \times I + V_{drop}^0 \quad (8)$$

$$P_{max} = \frac{(V - V_{drop}^0)^2}{4R_s} \quad (9)$$

Here, the specific capacitance, the specific energy and the specific power only consider the weight of the active material in the electrode. In the two-electrode system, m is the total mass of two electrode active materials.

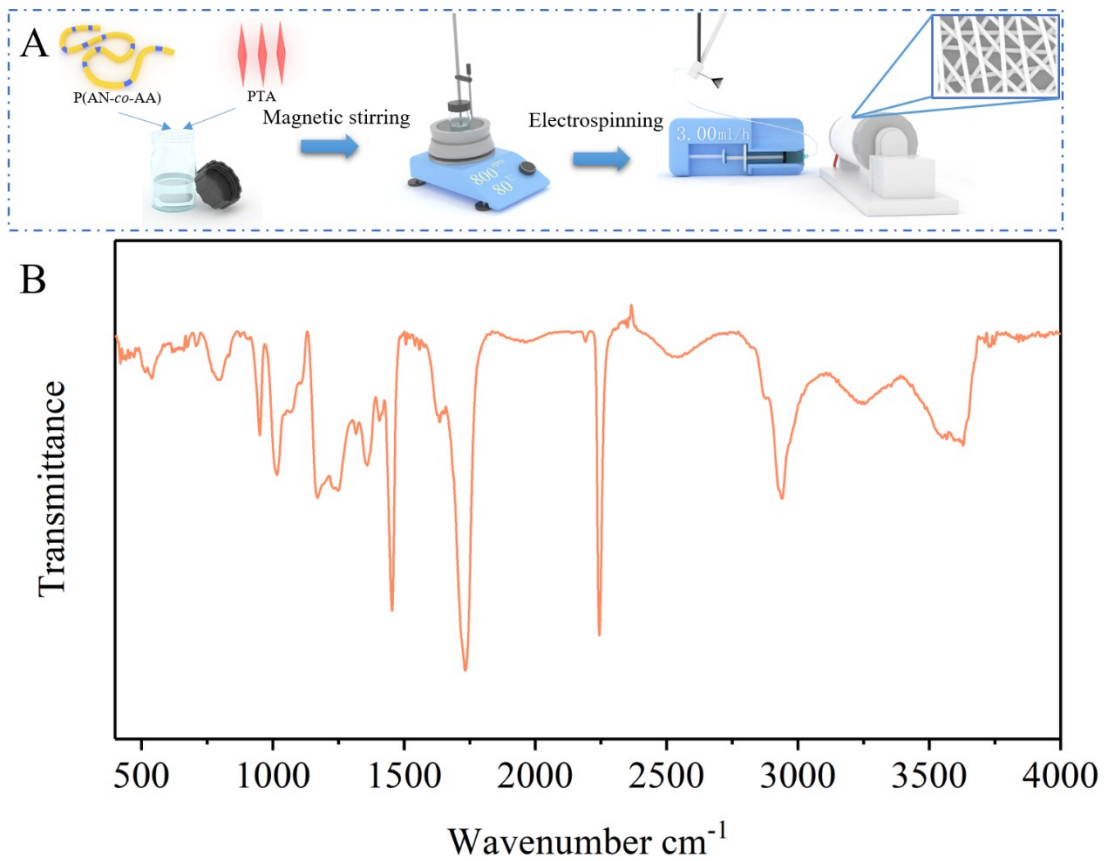


Fig. S1 A. Schematic diagram of P (AN-*co*-AA) / PTA fiber preparation process. **B.** FT-IR spectrum of P(AN-*co*-AA).

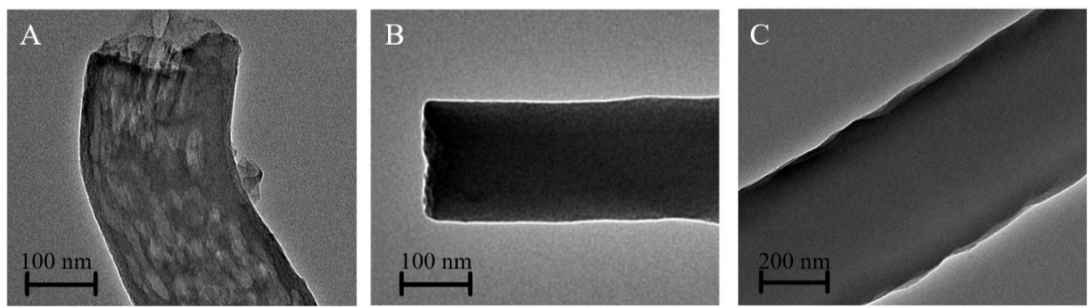


Fig. S2 TEM images of B-CNF(A), C-CNF (B) and fiber which formed without sublimating PTA (C).

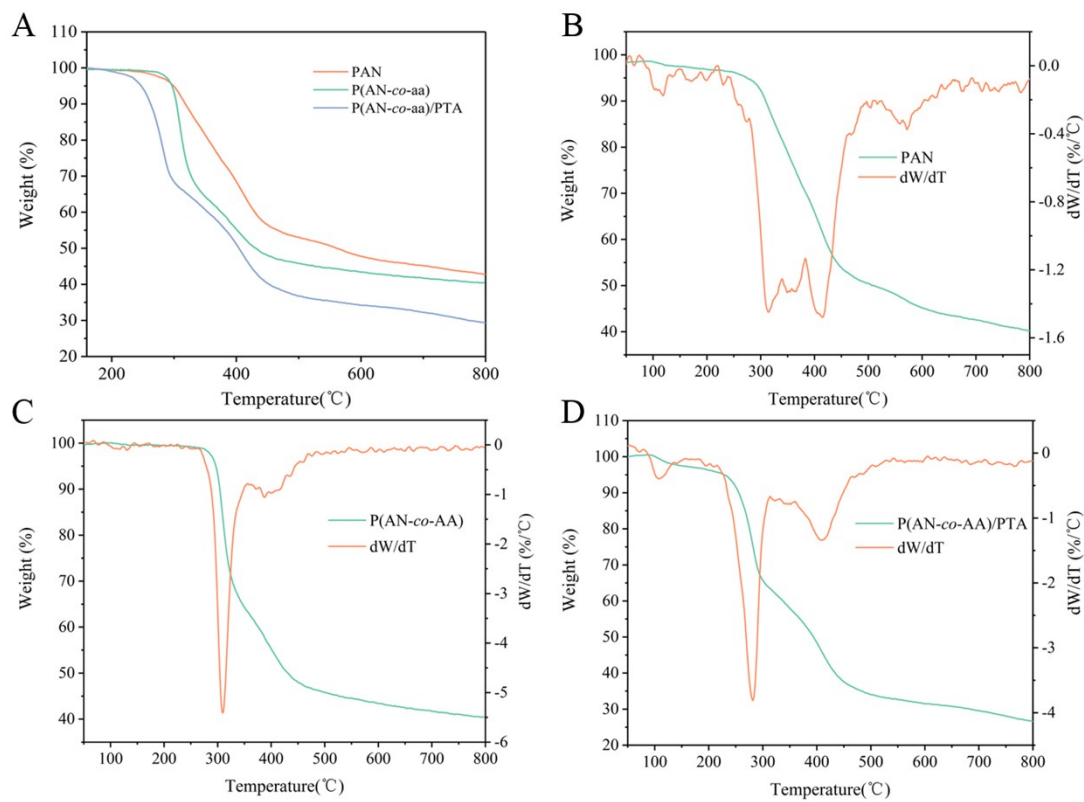


Fig. S3. Thermogravimetric analysis. **A.** Thermogravimetric analysis (TGA) and the first derivative (labeled as dW/dT) of the weight losses during the pyrolysis of **(B)** PAN, **(C)** P(AN-*co*-AA) and **(D)** P(AN-*co*-AA) / PTA. In order to eliminate the interference of residual DNF in the fiber. We choose 160 °C as the starting temperature for comparison.

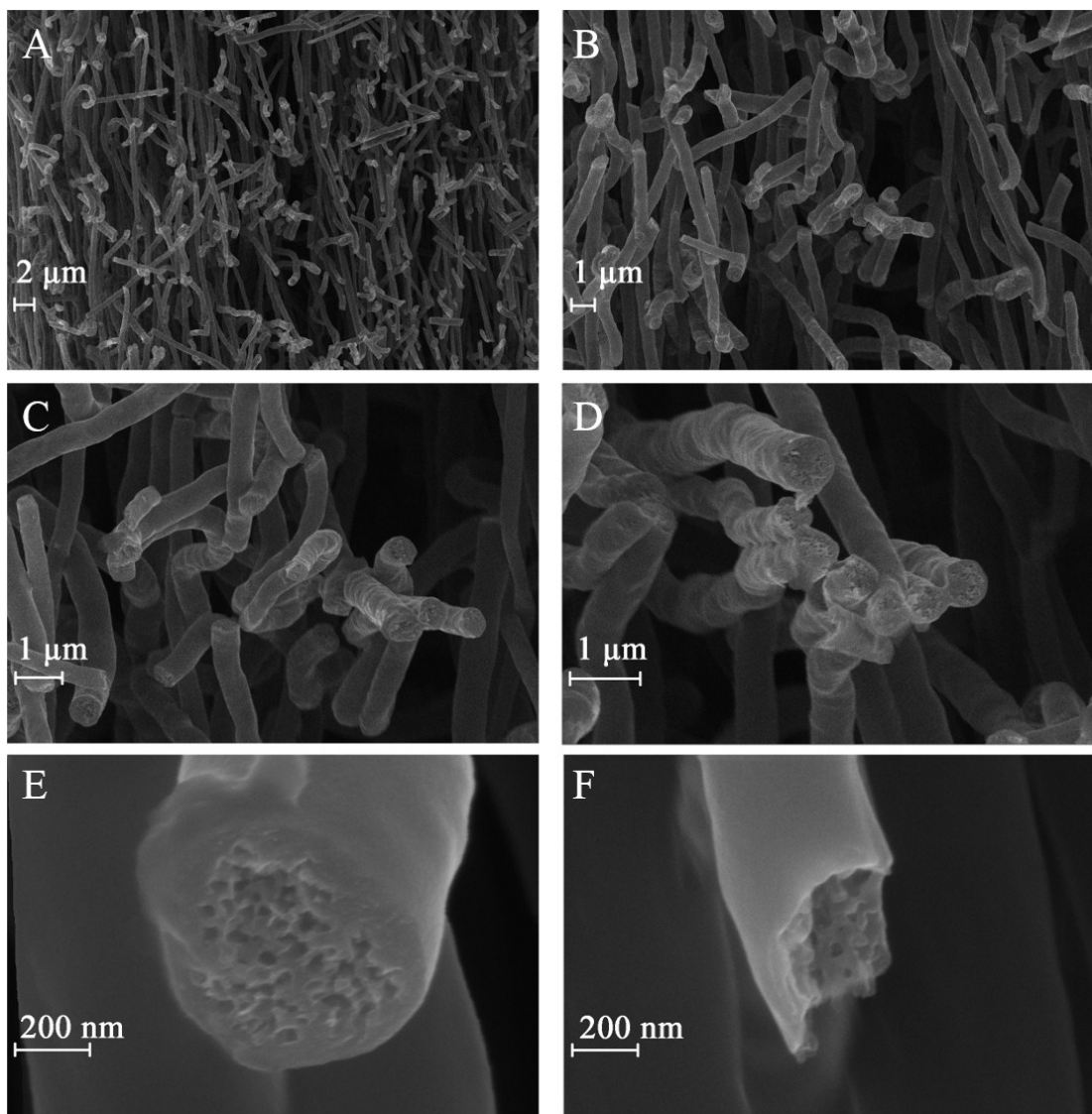


Fig. S4. Additional SEM images of HPCNFs. SEM images of HPCNFs after shearing (A-F).

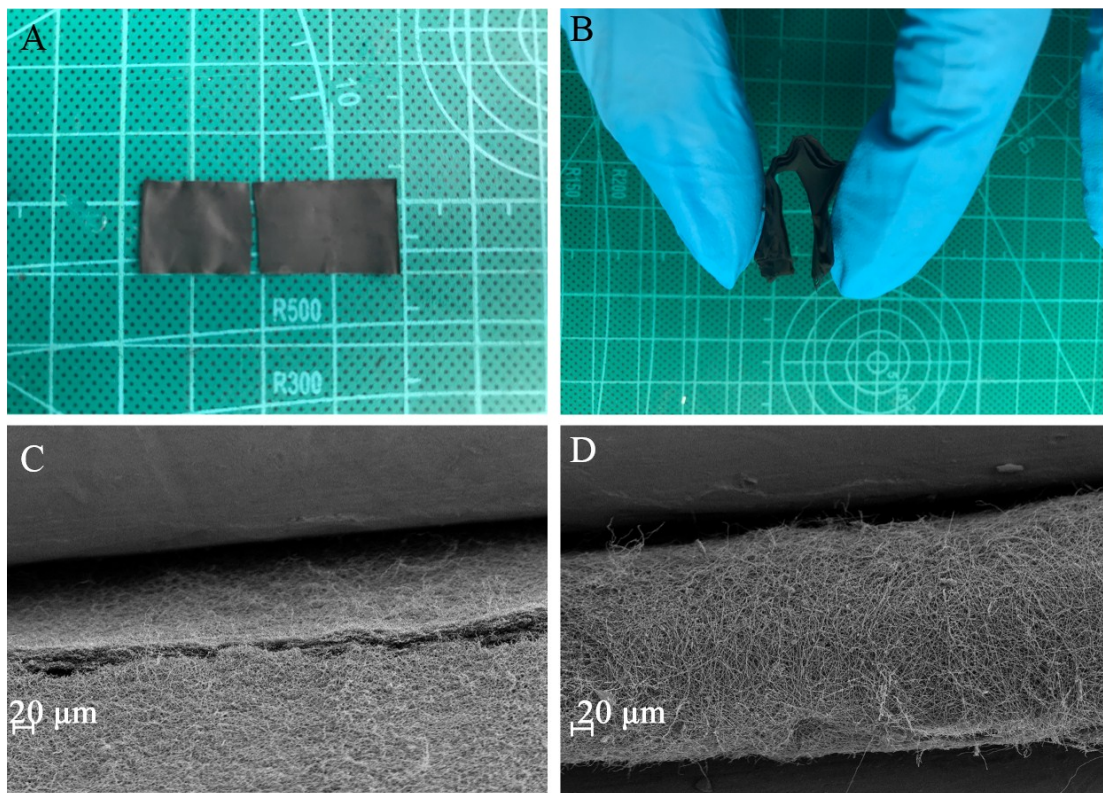


Fig. S5. Flexibility of HPCNFs. **A.** A photograph of a piece of C-CNFs. **B.** A photograph of a piece of HPCNFs. **C.** SEM image of C-CNFs. **D.** SEM image of C-CNFs.

C-CNFs break after simple bending and cracks between fibers can be clearly seen by SEM. HPCNFs can be bent at any angle. Even if the fiber felt is bent 180°, it cannot break the integrity of the fiber.

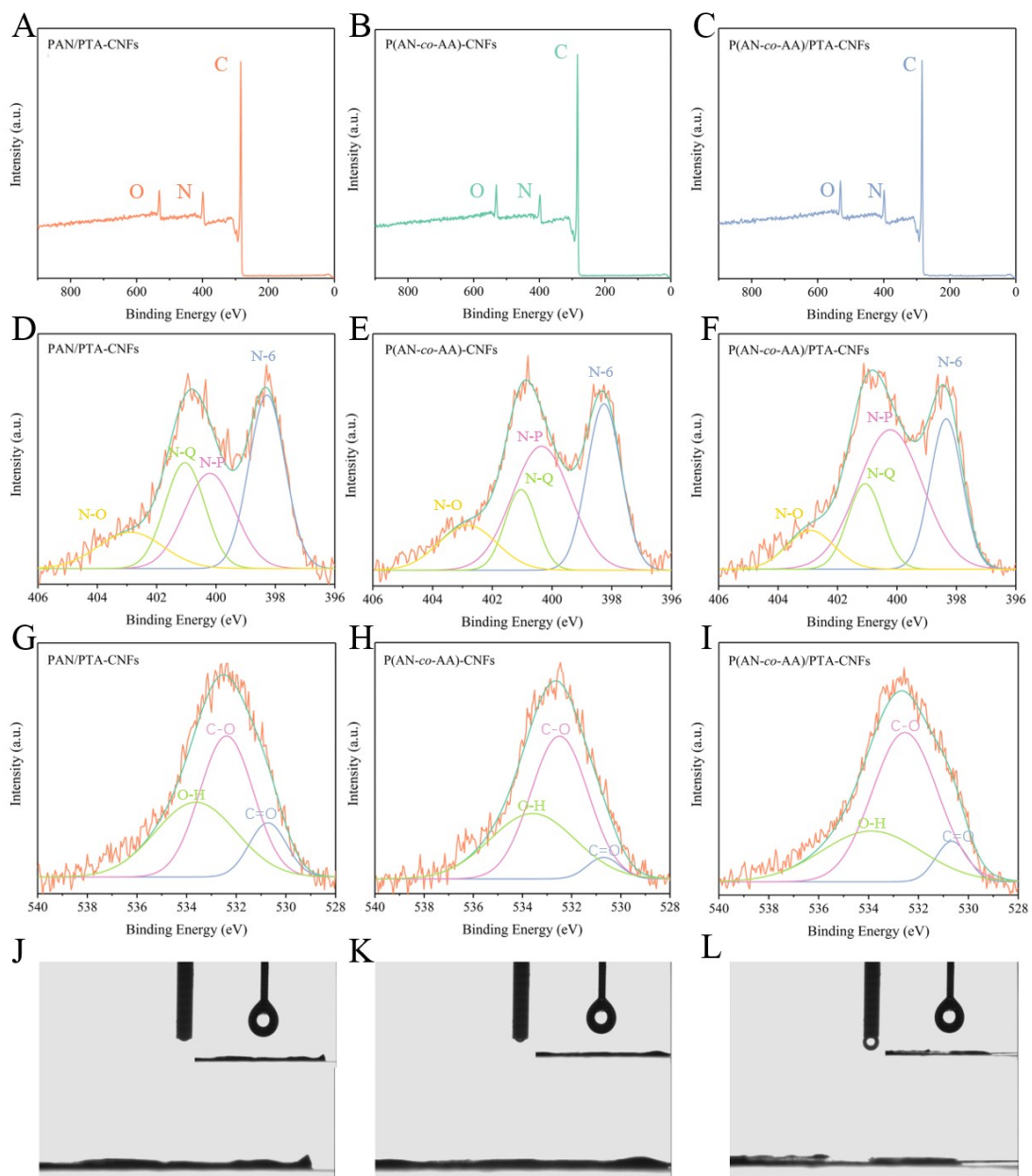


Fig. S6. XPS spectra and contact angles. XPS survey spectra of (A) B-CNFs, (B) C-CNFs, and (C) HPCNFs. XPS N 1s peaks of (D) B-CNFs, (E) C-CNFs, and (F) HPCNFs. XPS O 1s peaks of (G) B-CNFs, (H) C-CNFs, and (I) HPCNFs. Contact angles of (J) B-CNFs, (K) C-CNFs, and (L) HPCNFs after pyrolysis at 800 °C. The fluid used for testing was water.

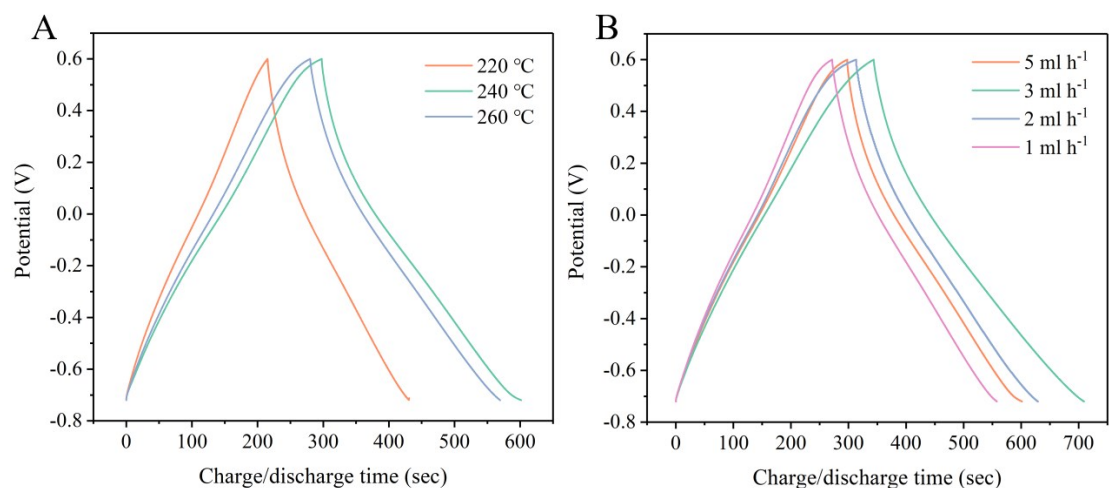


Fig. S7. Galvanostatic charge/discharge curves (1A g-1) of HPCNFs at different pre-oxidation temperature (A) and different spinning speed (B).

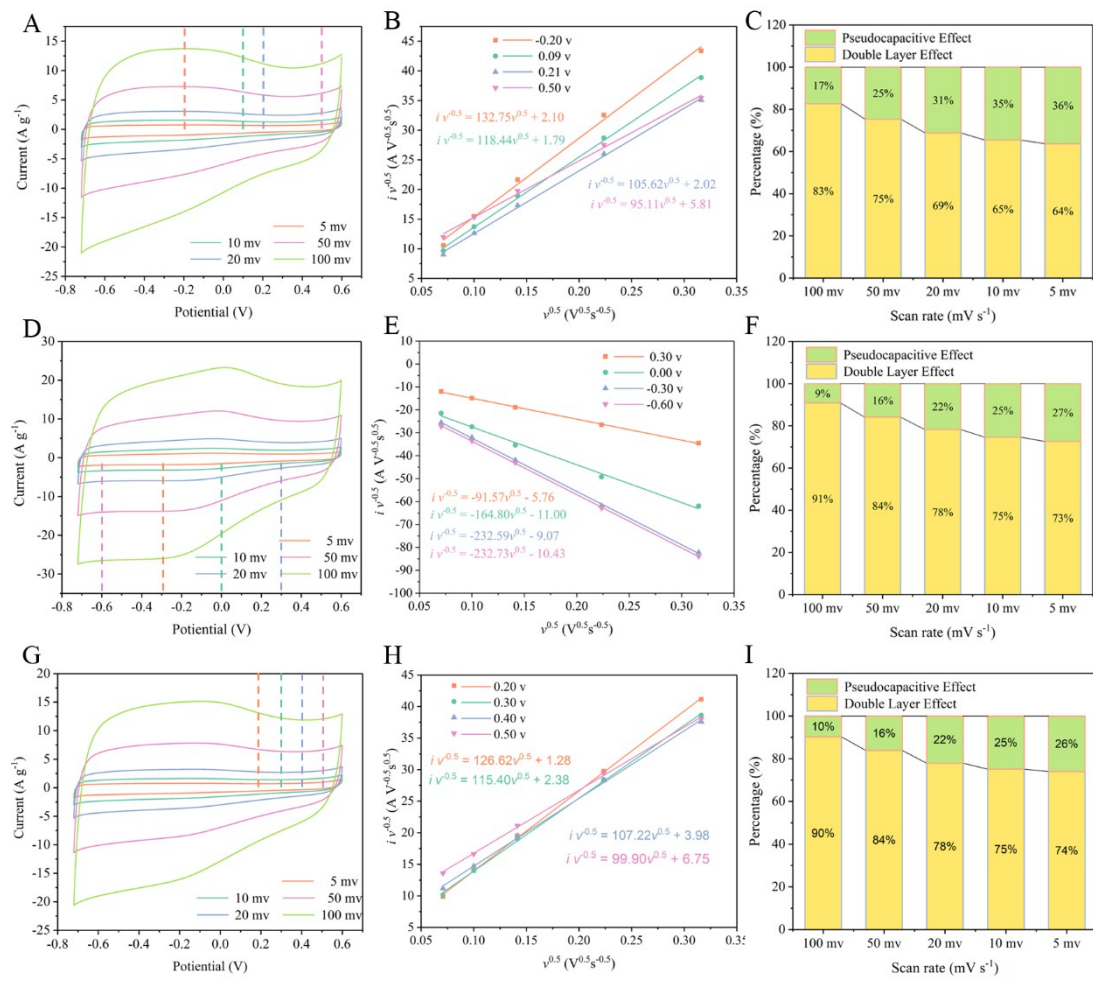


Fig. S8. Capacitance contribution analyses. **A.** CV curves at a sweep rate increase from 5 mV s⁻¹ to 100 mV s⁻¹ of B-CNFs. **B.** Dunn's method analysis: $iv^{0.5}$ vs. $v^{0.5}$ plot for B-CNFs using the anodic current at different potentials. **C.** Histograms of the capacitance contributions by the different processes of B-CNFs (Yellow, fast-kinetic processes; green, slow-kinetic processes). **D.** CV curves at a sweep rate increase from 5 mV s⁻¹ to 100 mV s⁻¹ of HPCNFs. **E.** Dunn's method analysis: $iv^{0.5}$ vs. $v^{0.5}$ plot for B-CNFs using the anodic current at different potentials. **F.** Histograms of the capacitance contributions by the different processes of HPCNFs (Yellow, fast-kinetic processes; green, slow-kinetic processes). **G.** CV curves at a sweep rate increase from 5 mV s⁻¹ to 100 mV s⁻¹ of C-CNFs. **H.** Dunn's method analysis: $iv^{0.5}$ vs. $v^{0.5}$ plot for C-CNFs using the anodic current at different potentials. **I.** Histograms of the capacitance contributions by the different processes of C-CNFs (Yellow, fast-kinetic processes; green, slow-kinetic processes).

We used Dunn's method to quantify the capacitance contribution from fast-kinetic processes (including electrical double layer capacitive processes and fast redox reactions) and slow-kinetic processes (redox reactions that are diffusion-controlled). First, the current density at a fixed potential and a scan rate, i was extracted from the CV curves. The current density (i) from the CVs can be expressed as a combination of two terms,

$$i = k_1 + k_2 v^{0.5} \quad (10)$$

The first term k_1 represents fast-kinetic processes and the second term $k_1 v^{0.5}$ represents slow-kinetic processes. Dividing $v^{0.5}$ on both sides of the equation yields

$$iv^{-0.5} = k_1 v^{-0.5} + k_2 \quad (11)$$

Therefore, by reading i from the CVs at a series of scan rates and then plotting $iv^{0.5}$ vs. $v^{0.5}$, one expects to obtain a linear fitting line with a slope of k_1 and a y-intercept of k_2 . Calculate the capacitance contribution of material using k_1 plotting

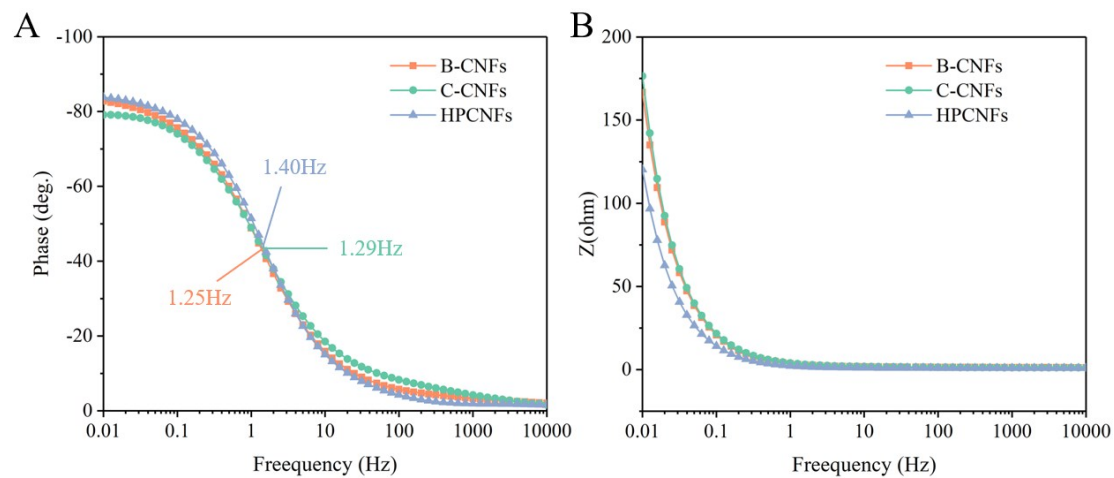


Fig. S9. Impedance analysis. A. Phase angle Bode plot of B-CNFs, C-CNFs, and HPCNFs. **B.** The plot of total impedance versus frequency of B-CNFs, C-CNFs, and HPCNFs.

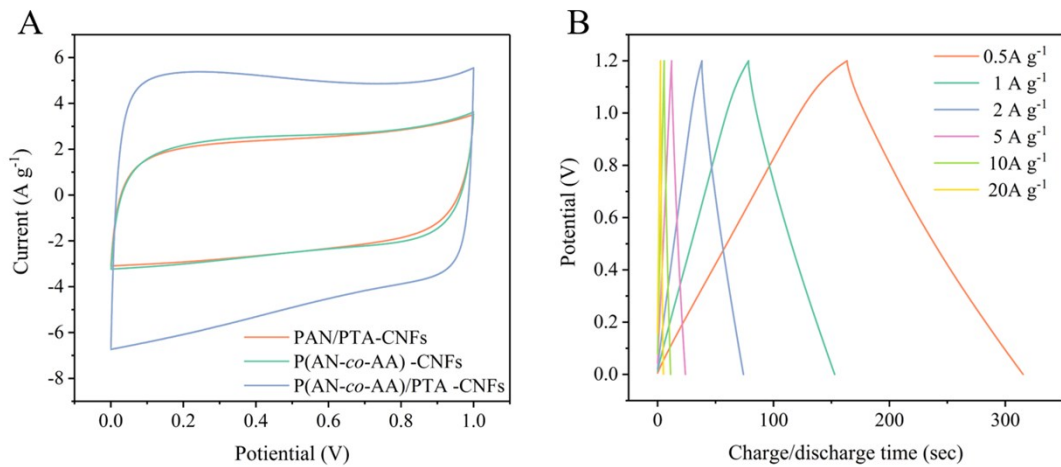


Fig. S10. Electrochemical performance **A.** Cyclic voltammogram curves (100 mV s^{-1}) for different CNFs. **B.** Galvanostatic charge/discharge (GCD) curves of ACNF-12 at different current densities,

Table S1. The content of the elements in the copolymer.

Molar ratio	Element content wt%		
	C	N	H
P(AN-co-AA)	63.34	21.957	5.752

Table S2. Summary of the physical and chemical characterization.

Characterizations		B-CNFs	C-CNFs	HPCNFs
BET	S_{BET} (m^2/g)	277.5	302.7	406.0
	BJH Adsorption average pore radius (nm)	9.4	2.5	4.9
	BJH Desorption average pore radius (nm)	12.5	2.89	3.7
	Total pore volume (cm^3/g)	0.203	0.179	0.265
	Micropore volume (cm^3/g)	0.124	0.130	0.140
	Mesopore volume (cm^3/g)	0.075	0.049	0.125
Raman	D band center (nm)	1355	1357	1356
	G band center (nm)	1582	1583	1586
	I band center (nm)	1199	1200	1198
	A band center (nm)	1507	1502	1506
	D' band center (nm)	1618	1614	1612
	I_A/I_G	0.85	0.43	0.48
	$I_D/I_{D'}$	4.85	6.86	6.79
	I_D/I_G	2.45	3.21	3.26
C (%)		87.08	87.58	85.53
N (%)		8.11	7.18	8.48
O (%)		4.8	5.23	5.99
XPS	N-6	B.E. (eV)	398.28	398.26
		Content (%)	2.88	2.26
	N-P	B.E. (eV)	400.21	400.35
		Content (%)	2.20	2.86
	N-Q	B.E. (eV)	401.04	401.04
		Content (%)	1.94	1.02
	N-O	B.E. (eV)	402.88	402.82
		Content (%)	1.09	1.04
	C=O	B.E. (eV)	530.7	530.7
		Content (%)	0.62	0.26
	C-O	B.E. (eV)	532.4	532.4
		Content (%)	2.32	2.97
	O-H	B.E. (eV)	533.6	533.4

	Content (%)	1.85	2.01	1.88
Electrical Properties	Equivalent series resistance R_s (ohm)	1.23	1.12	0.833
	Charge transfer resistance R_{ct} (ohm)	0.189	0.269	0.0698
	Diffusion resistivity σ (ohm s ^{0.5})	2.96	3.59	1.64
	Ion diffusion resistance W_0 (S s ^{0.5})	0.288	0.247	0.559
	CPE1 Coefficient Y (S s ^a)	0.00815	0.0137	0.00920
	Exponent a	0.73	0.78	0.71
	CPE2 Coefficient Y (S s ^a)	0.085	0.077	0.12
	Exponent a	0.99	0.98	0.99

Table S3. Summary of the electrochemical capacitive performance of HPCNFs electrodes to generate the charts in Fig. 3. Note: 1) For fair comparison, the capacitances are all evaluated at 0.5A g⁻¹. 2) For fair comparison of fibrous electrodes, the table only includes capacitances of carbon fibers. 3) The porous carbon fibers in this work are not activated, which can be done easily to further improve the performance.

Electrode materials	Precursors	Activation agent	Specific Surface area (m ² g ⁻¹)	Gravimetric capacitance (F g ⁻¹ , 0.5A g ⁻¹)	BET-area-normalized capacitance (μF cm ⁻²)	references
Porous flexible						
carbon nanofiber	Phenolicresin/poly(vinyl alcohol) (PVA)	KOH	1317	~250	18	1
(CNF) paper						
CNFs with radially grown graphene sheets						
porous carbon fibers	PAN/graphene	NH ₃	2185	133	6	2
3D hierarchical						
porous carbon fibers	PAN	HCl	2177	~270	12	3
Graphene integrating carbon fibers						
activated carbon fibers	PAN/graphene	KOH	830	150 (5mv/s)	18	4
Nomex-derived Nomex aramid fibers						
mesoporous CNFs	PAN	Mg(OH) ₂	926	327	35.3	6
Plasma oxidized PAN						
		Plasma	274	~200 (5mv/s)	73	7

electrospun CNFs							
Activated carbon fiber webs	Poly(amic acid) (PAA)	Water steam	2100	175	8.3	8	
Porous CNFs	PAN/PMMA	CO ₂	2419	140	5.8	9	
Porous CNFs	PAN	ZnCl ₂	550	140	25.5	10	
Activated porous CNFs using Sn	PAN/poly(viny lpyrrolidone) (PVP)	Sn/Acid	1082	289 (10mVs ⁻¹)	26.7	11	
Nitrogen-doped hierarchical porous carbon fibers	PAN/PMMA/ tetraethyl orthosilicate/ thermoplastic polyurethane	HF acid/SiO ₂	1126	203	18.0	12	
Nitrogen-doped hollow activated CNFs	PAN/PVP	NH ₃	701	~190	27.1	13	
Graphitic carbon nitride nanosheets @ N-enriched mesoporous CNFs	PAN/g-C ₃ N ₄ nanosheets	Water steam	554	~200	36.1	14	
High surface- area CNFs	Synthesized polymer (PIM-1)	Water steam	1162	149	12.8	15	
N/P/K co-doped porous CNFs	Cane molasses	/	580	171	29.5	16	
Heteroatom- enriched electrospun	Melamine formaldehyde resin/PVA	/	320	206	64	17	

CNFs						
Electrospun						
	PAN/graphene	/	480	183	38.1	18
CNFs/graphene						
CNF/CNT composite	PAN/CNT/spherical latex nanoparticles	/	535	235	43.9	19
CNFs	Poly(amideimide)	/	1360	150	13.5	20
Microporous CNFs	Phenolic resin/TEOS/PvP	/	2164	~310	14.3	21
Microporous CNFs	PAA/PVP	/	804	~190	23.75	22
Nitrogen-enriched porous CNFs	PAN/allylpolyethylene neglycol (PEG)	/	753	~280	37.2	23
Porous CNTs(55)	Polyaniline nanotubes	/	3253	~320	9.8	24
ZnCl ₂ -activated and filter paper-derived CNFs	Waste filter paper	ZnCl ₂	2232	302	13.5	25
ultra-thin carbon nanofibers						
Hierarchical porous carbon fibers	PAN/SiO ₂	KOH	1632	197 (5mVs ⁻¹)	12	27
carbon nanofiber	PAN	KOH	1220	175	14.3	28
nanoporous ultrafine carbon fibers						
Zinc oxide/activated carbon	PAN/zinc acetate	steam	1404	178	12.7	30

nanofiber						
carbon nanofiber	PAN	CO ₂	375	240	64	31
Carbon nanofiber	PAN	steam	1120	112	10	32
Carbon nanofiber	PAN	steam	1230	175	14.2	33
porous carbon nanofibers	PAN/Na ⁺ ion		1600	210 (1A g-1)	13.1	34
mesoporous						
carbon nanofiber	PAN/Mg(NO ₃) ₂		674	270	40	35
hierarchical						
porous carbon nanofiber	PAN/ PMMA/SiO ₂		699	170	24.2	36
porous carbon nanofiber	PAN/ PTA		1144	257	22.5	37
Hierarchical fibers						
porous carbon fibers	P(AN-b-AA)		503	360	66	38

References

1. C. Ma, Y. Li, J. Shi, Y. Song and L. Liu, *Chem. Eng. J.*, 2014, **249**, 216-225.
2. L. Zhao, Y. Qiu, J. Yu, X. Deng, C. Dai and X. Bai, *Nanoscale*, 2013, **5**, 4902-4909.
3. Y. Li, C. X. Lu, S. C. Zhang, F. Y. Su, W. Z. Shen, P. C. Zhou and C. L. Ma, *J. Mater. Chem. A*, 2015, **3**, 14817-14825.
4. H. N. Zhang, A. N. Li, J. Wang, Y. Zhang, Z. Zhao, H. F. Zhao, M. Cheng, C. W. Wang, J. Y. Wang, S. C. Zhang and J. Z. Wang, *Carbon*, 2018, **126**, 500-506.
5. K. Leitner, A. Lerf, M. Winter, J. O. Besenhard, S. Villar-Rodil, F. Suárez-García, A. Martínez-Alonso and J. M. D. Tascón, *J. Power Sources*, 2006, **153**, 419-423.
6. J. Tan, Y. L. Han, L. He, Y. X. Dong, X. Xu, D. N. Liu, H. W. Yan, Q. Yu, C. Y. Huang and L. Q. Mai, *J. Mater. Chem. A*, 2017, **5**, 23620-23627.
7. C. C. Lai and C. T. Lo, *RSC Adv.*, 2015, **5**, 38868-38872.
8. C. Kim, Y. O. Choi, W. J. Lee and K. S. Yang, *Electrochim. Acta*, 2004, **50**, 883-887.
9. N. C. Abeykoon, J. S. Bonso and J. P. Ferraris, *RSC Adv.*, 2015, **5**, 19865-19873.
10. C. Kim, B. T. N. Ngoc, K. S. Yang, M. Kojima, Y. A. Kim, Y. J. Kim, M. Endo and S. C. Yang, *Adv. Mater.*, 2007, **19**, 2341-2346.
11. G. H. An and H. J. Ahn, *Carbon*, 2013, **65**, 87-96.
12. J. Zeng, C. Qi, X. Y. Wang, J. Bo, X. X. Peng and X. L. Tang, *J. Solid State Electrochem.*, 2015, **19**, 1591-1597.
13. Q. Xu, X. L. Yu, Q. H. Liang, Y. Bai, Z. H. Huang and F. Y. Kang, *J. Electroanal. Chem.*, 2015, **739**, 84-88.
14. Q. H. Liang, L. Ye, Q. Xu, Z. H. Huang, F. Y. Kang and Q. H. Yang, *Carbon*, 2015, **94**, 342-348.

15. J. S. Bonso, G. D. Kalaw and J. P. Ferraris, *J. Mater. Chem. A*, 2014, **2**, 418-424.
16. A. Kurniawan, L. K. Ong, F. Kurniawan, C. X. Lin, F. E. Soetaredjo, X. S. Zhao and S. Ismadji, *RSC Adv.*, 2014, **4**, 34739-34750.
17. C. Ma, Y. Song, J. Shi, D. Zhang, Q. Guo and L. Liu, *J Colloid Interface Sci*, 2013, **395**, 217-223.
18. Q. Dong, G. Wang, H. Hu, J. Yang, B. Q. Qian, Z. Ling and J. S. Qiu, *J. Power Sources*, 2013, **243**, 350-353.
19. Y. Zeng, X. Y. Li, S. H. Jiang, S. J. He, H. Fang and H. Q. Hou, *Mater. Lett.*, 2015, **161**, 587-590.
20. M. K. Seo and S. J. Park, *Materials Science & Engineering B*, 2009, **164**, 106-111.
21. J. Sheng, C. Ma, Y. Ma, H. X. Zhang, R. R. Wang, Z. Y. Xie and J. L. Shi, *Int. J. Hydrogen Energy*, 2016, **41**, 9383-9393.
22. T. Le, Y. Yang, Z. H. Huang and F. Y. Kang, *J. Power Sources*, 2015, **278**, 683-692.
23. K. B. Huang, L. Min, Z. H. Chen, Y. Y. Yao and X. W. Yang, *Electrochim. Acta*, 2015, **158**, 306-313.
24. T. T. Zhu, J. Zhou, Z. H. Li, S. J. Li, W. J. Si and S. P. Zhuo, *J. Mater. Chem. A*, 2014, **2**, 12545.
25. B. B. Chang, Y. Z. Guo, Y. C. Li and B. C. Yang, *RSC Adv.*, 2015, **5**, 72019-72027.
26. W. M. Chang, C. C. Wang and C. Y. Chen, *Electrochim. Acta*, 2019, **296**, 268-275.
27. D. Y. Lee, J. Y. Jung, M. J. Jung and Y. S. Lee, *Chem. Eng. J.*, 2015, **263**, 62-70.
28. C. Kim, S. H. Park, W. J. Lee and K. S. Yang, *Electrochim. Acta*, 2004, **50**, 877-881.

29. C. Ma, J. N. Chen, Q. C. Fan, J. C. Guo, W. N. Liu, E. Cao, J. L. Shi and Y. Song, *J. Mater. Sci.*, 2017, **53**, 4527-4539.
30. C. H. Kim and B. H. Kim, *J. Power Sources*, 2015, **274**, 512-520.
31. E. J. Ra, E. Raymundo Piñero, Y. H. Lee and F. Béguin, *Carbon*, 2009, **47**, 2984-2992.
32. K. H. Jung, W. Deng, D. W. Smith and J. P. Ferraris, *Electrochem. Commun.*, 2012, **23**, 149-152.
33. C. Kim and K. S. Yang, *Appl. Phys. Lett.*, 2003, **83**, 1216-1218.
34. C. Tran and V. Kalra, *J. Power Sources*, 2013, **235**, 289-296.
35. C. Ma, J. Sheng, C. Ma, R. Wang, J. Liu, Z. Xie and J. Shi, *Chemical Engineering Journal*, 2016, **304**, 587-593.
36. Q. Wang, Q. Cao, B. Jing, H. Kuang and L. Zhou, *J. Solid State Electrochem.*, 2013, **17**, 2731-2739.
37. Y. L. Cheng, L. Huang, X. Xiao, B. Yao, Z. M. Hu, T. Q. Li, K. Liu and J. Zhou, *J. Power Sources*, 2016, **327**, 488-494.
38. Z. P. Zhou, T. Y. Liu, A. U. Khan and G. L. Liu, *Sci. Adv.*, 2019, **5**, eaau6852.